# Hydrogen embrittlement of a bimaterial

C. Ayas, N.A. Fleck, V.S. Deshpande*

*Department of Engineering, Cambridge University, Trumpington Street, Cambridge CB2 1PZ, UK.*

**Abstract**

Commonly, within the energy industry, the corrosion resistance of pressure vessel steels is increased by the addition of an overlay coating comprising a nickel-based alloy or a stainless steel. However, the interface between the two alloys is prone to hydrogen-assisted cracking, due to for example carbide precipitation near the interface. In the present study, the sensitivity of the tensile strength of the interface to hydrogen concentration is measured for both notched and un-notched specimens made from the overlay welding of 690 nickel alloy on a low alloy steel A533B. An elastic-plastic finite element analysis is used to determine the stress and strain state near the notch root, and thereby to calculate the local distribution of hydrogen within the lattice and at traps. The observed strength of the notched specimens is best rationalised by assuming that the local cohesive strength of the interface is a function of the lattice hydrogen concentration, with a negligible influence of the trapped hydrogen. The scatter in specimen strength, and the relative strength of the notched and un-notched specimens, are adequately described by Weibull statistics, with a low value of Weibull modulus equal to 3.4.

*Keywords:* Failure, hydrogen, diffusion, size effects.

## 1. Introduction

Weld cladding is the deposition of a relatively thick (3 mm or more) metal layer onto a metallic substrate in order to improve the corrosion or wear resistance of the material. It is widely used in nuclear and steam power plants, petrochemical applications and in pipelines (Rao et al., 2011). An

*Corresponding author *E-mail address:* vsd@eng.cam.ac.uk

example is the overlay of stainless steel on the surface of a low alloy steel for improved corrosion resistance.

Usually, the clad and the base material are metals of dissimilar composition and properties, and it is challenging to produce a dissimilar welding interface that is of sufficient strength and ductility that the component will not fail from the weld (Satyanarayana et al., 2005). Intermetallic compounds may form at the weld interface between the dissimilar metals that deteriorate ductility, or increase susceptibility to corrosion or hydrogen embrittlement (Sireesha et al., 2000). The weld strength can also be significantly degraded by the presence of residual stress. For example, Lee and Chang (2012) have presented a three-dimensional FE simulation of bimaterial welding to identify the temperature and residual stress fields in butt-welded joints between plain carbon steels and stainless steels.

Hydrogen embrittlement is a recognised threat for welded joints since hydrogen take-up can arise during the welding operation. Recently, Blach et al. (2011) have investigated the influence of hydrogen charging upon the room temperature tensile properties and fracture behaviour of dissimilar welded joints. They conjectured that hydrogen charging has a detrimental effect upon the strength of a ferritic/ferritic weld, but only a small influence on the strength of a ferritic/austenitic weld.

In our previous work (Ayas et al., 2013) we investigated the hydrogen embrittlement of monolithic, high strength low alloy AISI 4135 steel; we concluded that strength of notched and un-notched specimens correlate with the concentration of lattice (diffusible) hydrogen while the trapped hydrogen at dislocations, grain boundaries and carbides have a negligible effect on the failure strength. A fracture locus for notched specimens was established in terms of peak maximum principal stress versus concentration of diffusible hydrogen. A similar fracture locus, but displaced to lower strength levels, was obtained for un-notched specimens. Weibull theory was used to account for the reduction in strength with increasing stressed-volume.

In the current paper, we measure and analyse the loss in strength of a dissimilar weld, comprising 690 Nickel alloy and A533B low alloy steel (LAS) for pressure vessel applications, due to dissolved hydrogen. A failure locus in terms of strength versus hydrogen content is constructed for both notched and un-notched specimens, and Weibull theory is invoked in order to account for the observed statistical scatter in strength and for an observed size effect.

## 2. A brief summary of Oriani theory

We begin our study by summarising the relative distribution of hydrogen in the lattice and at traps, in accordance with Oriani's theory (Oriani, 1970; Sofronis and McMeeking, 1989). Hydrogen is stored either at normal interstitial lattice sites (NILS) or is trapped at micro-structural defects such as dislocations, grain boundaries, interfaces and carbides. The concentration of hydrogen at NILS, also called the lattice hydrogen concentration, is given by

$$C_L = \theta_L \beta N_L, \tag{1}$$

where $\theta_L$ is the fraction of occupied interstitial lattice sites, $\beta$ is the number of NILS per lattice atom and $N_L$ is the number of lattice atoms per unit volume. Similarly, the concentration of hydrogen trapped at any given site is

$$C_T = \theta_T \alpha N_T, \tag{2}$$

where $\theta_T$ is the fraction of occupied trapping sites, $\alpha$ is the number of atom sites per trap and $N_T$ is the number of traps per unit volume. Oriani's equation relates the equilibrium value of occupancy ratio of sites, in terms of an equilibrium constant $K$, as

$$\frac{\theta_T}{1-\theta_T} = K \frac{\theta_L}{1-\theta_L}. \tag{3}$$

In turn, $K$ is related to the the trap binding energy $\Delta H$, the gas constant $R = 8.314$ J/(mol K) and the absolute temperature $T$ according to

$$K = \exp\left(\frac{-\Delta H}{RT}\right). \tag{4}$$

Upon examining Eq. (4) we recognise that the value of $\theta_T$ is much more sensitive to $\Delta H$ than to $\theta_L$ since the equilibrium constant $K$ has an exponential dependence upon $\Delta H$.

### *2.1. Dislocation traps*

Now consider dislocation traps. The concentration of hydrogen $C_T^{(\mathrm{d})}$ trapped at dislocation cores is given by Eq. (2), with $\alpha = 1$, and $\theta_T$ given by Eqs. (3) and (4). However, the number of dislocation traps per unit volume $N_T^{(d)}$ increases with the von Mises plastic strain $\varepsilon^{\mathrm{p}}$ in contrast to the fixed

number of carbide traps $N_T^{(c)}$ and grain boundary traps $N_T^{(\mathrm{gb})}$. Following Novak et al. (2010) we can relate $N_T^{(\mathrm{d})}$ to the dislocation density $\rho_d$ and to the lattice parameter $a$ of the crystal structure of host atoms according to

$$N_T^{(\mathrm{d})} = \sqrt{2}\rho_{\mathrm{d}}/a. \tag{5}$$

In turn, $\rho_d$ scales with $\varepsilon^{\mathrm{p}}$ according to

$$\rho_d = \begin{cases} \rho_0 + k\varepsilon^{\mathrm{p}} & \varepsilon^{\mathrm{p}} \leq 0.5 \\ 10^{16}\mathrm{m}^{-2} & \varepsilon^{\mathrm{p}} > 0.5 \end{cases} \tag{6}$$

where $\rho_0 = 10^{10}$ m$^{-2}$ is the dislocation density of the material at zero plastic strain and $k = 2 \times 10^{16}$ m$^{-2}$ (Novak et al., 2010). The set of equations (1-6) gives the concentration of hydrogen $C_T^{(\mathrm{d})}$ that is trapped at dislocations. In order to specify the value of $C_T^{(\mathrm{d})}$, the values of ($\varepsilon^{\mathrm{p}}$, $C_L$) and the binding energy for dislocation traps $\Delta H^{(\mathrm{d})}$ need to be determined. In general, $\varepsilon^{\mathrm{p}}$ is known as function of loading history and position. For example, it is known immediately for an un-notched specimen under uniaxial tension, and can its spatial distribution be deduced from an elastic-plastic FE analysis for a notched specimen. The lattice concentration $C_L$ is generally determined experimentally by thermal desorption spectroscopy (TDS), along with a knowledge of the local hydrostatic stress distribution $\sigma_h$, as discussed below. However, the value for $\Delta H^{(\mathrm{d})}$ is problematic as the values quoted in the literature range from $\Delta H^{(\mathrm{d})} = -18$ kJ/mol (Novak et al., 2010) to $\Delta H^{(\mathrm{d})} = -36.4$ kJ/mol (Oriani, 1970). In order to bound the predicted behaviour, we shall calculate the dislocation-trapped hydrogen concentration $C_T^{(\mathrm{d})}$ using two extreme values of $\Delta H^{(\mathrm{d})}$, namely -18 kJ/mol and -36.4 kJ/mol.

## 3. The hydrogen concentration in a notched specimen

Commonly, the sensitivity of a material to hydrogen embrittlement is determined by performing notched/un-notched tensile tests on specimens that have been either pre-charged or are continuously charged with hydrogen during the test. In this section, we outline a simple scheme for determining the distribution of hydrogen in a notched specimen that is charged continuously under remote tension. First, consider a sample under zero applied stress that is in contact with a charging environment such that the hydrogen equilibrium has been established. Thermodynamic equilibrium dictates that the chemical potential of hydrogen to remain spatially uniform within the specimen.

Consequently, the chemical potential of hydrogen in the specimen can be written as

$$\mu = \mu_0 + RT \ln C_L^0, \tag{7}$$

where $\mu$ is the chemical potential in the charging environment, $\mu_0$ is the chemical potential in the standard state and $C_L^0$ is the uniform lattice hydrogen concentration in the unstressed sample. Now consider a notched bar that is placed in the charging environment and simultaneously subjected to uniaxial tension at a sufficiently low rate that hydrogen equilibrium is maintained during the test. Then, the spatially uniform chemical potential of the notched specimen is now given by

$$\mu = \mu_0 + RT \ln C_L^0 = \mu_0 + RT \ln C_L(x_i) - \sigma_h(x_i) V_H, \tag{8}$$

where $\sigma_h$ and $C_L$ are the hydrostatic stress and hydrogen concentration, respectively at location $x_i$ and $V_H$ is the partial molar volume of hydrogen in solid solution. Suitable rearrangement of the above expression allows $C_L$ to be specified in terms of the local hydrostatic stress as

$$C_L(\sigma_h) = C_L^0 \exp\left(\frac{\sigma_h V_H}{RT}\right). \tag{9}$$

## 4. Strength measurements of dissimilar weld

A series of tensile tests have been performed on notched and un-notched bimaterial specimens, at selected values of hydrogen concentration. We begin by detailing the manufacture of the bimaterial specimens and then describe the method of hydrogen charging and the test method.

### *4.1. Specimen manufacture*

Tensile tests were performed on hydrogen-charged dog-bone specimens machined from a bimaterial plate of 690 alloy/A533B LAS. The gauge-section of the notched and un-notched dog-bone specimens are sketched in Fig. 1. The bimaterial plate was manufactured from a square plate of A533B LAS of side-length 100 mm and thickness 60 mm by overlay welding with 690 alloy to a thickness of 60 mm. The chemical composition of the 690 alloy in weight percent reads 0.038 C, 0.28 Si, 4.31 Mn, 29.14Cr, 0.08Ti, 8.54 Fe, 1.63 (Ta+Nb), 0.019 N, and remainder Ni, while the chemical composition of LAS in weight percent is 0.18 C, 0.25 Si, 1.46 Mn, 0.69 Ni, 0.15 Cr, 0.57

Mo, and remainder Fe. Prior to the overlay welding operation, the LAS was austenitized at 880°C for 185 minutes, and water-quenched to room temperature, tempered at 645°C for 380 minutes in order to achieve tempered martensite.

The bimaterial was produced by shielded, metal arc welding of 690 alloy rods, of diameter 4 mm, onto the LAS using a current of 140 A, voltage of 21 V and a welding speed of 2.7 mm $s^{-1}$. Subsequently, a post-weld heat treatment was applied by heating up the bimaterial to 615°C for 5 hours.

*4.2. Calibration of charging conditions for hydrogen*

The dog-bone specimens were immersed in a range of aqueous environments, and a prescribed current density was impressed in order to achieve an equilibrium concentration of hydrogen, see Table 1. The hydrogen concentration $C_L^0$ is measured by the standard technique of Thermal Desorption Spectroscopy (TDS), and is briefly summarised as follows. Test plates of LAS, of dimension 10 mm × 5 mm × 1 mm, were charged for 24 hours using each of the charging conditions listed in Table 1. This time is adequate to give an equilibrium concentration of hydrogen, in view of the fact that the room temperature diffusion constant for hydrogen within LAS is $D = 8.75 \times 10^{-11}$ $m^2$ $s^{-1}$. The TDS measurement consists of heating the test plate at 100°C/hour from room temperature to 600°C and recording the hydrogen desorption rate as a function of time (or equivalently temperature) via mass spectroscopy. It is assumed that the diffusible/lattice hydrogen is desorbed up to a temperature of 250°C, and consequently the value of $C_L^0$ is taken to be the area under the curve of desorption rate versus time up to a temperature of 250°C. (At higher temperatures, the hydrogen desorbs from the strong traps, such as grain and carbides).

*4.3. Test Method*

The bimaterial dog-bone specimens, of gauge section shown in Fig. 1, were pre-charged for 24 hours using the environments listed in Table 1. During this pre-treatment, the specimens were held under fixed load such that the net section stress $\sigma_{\text{net}}$ was 20MPa. After the pre-treatment, the imposed hydrogen environment was maintained and $\sigma_{\text{net}}$ was increased according to the prescription as sketched in Fig. 2:

(i) immediate increase to 100 MPa, then
(ii) increment $\sigma_{\text{net}}$ by 1.20 MPa every 900 s until failure occurs. Thus, the average loading rate is 1.3 kPa $s^{-1}$.

*4.4. Measured tensile strength as a function of hydrogen content*

The maximum net section stress (i.e. the failure stress) $\sigma_{\max}$ is plotted as a function of lattice hydrogen concentration $C_L^0$ in Fig. 3 for both the un-notched and notched specimens. For both geometries the following qualitative behaviour is observed. At $C_L^0$ below about 0.1 wppm, $\sigma_{\max}$ is almost independent of $C_L^0$ and has little scatter in value. In contrast, at $C_L^0$ above 0.1 wppm, $\sigma_{\max}$ drops with increasing $C_L^0$ and displays significant scatter. This is suggestive of a switch in failure mechanism. To investigate this, the fracture surfaces of the specimens were examined in the optical and scanning electron microscope (SEM).

Consider first the notched specimens. Failure was always along the weld interface; micro-void coalescence occurred at $C_L^0$ below about 0.1 wppm, whereas brittle, inter-granular failure occurred at higher values of $C_L^0$, compare the SEM image in Fig. 4a for $C_L^0 = 0.07$ wppm with that shown in Fig. 4b for $C_L^0 = 0.25$ wppm. Second, consider the un-notched specimens. The fracture surface of the severely charged specimens, at $C_L^0$ above 0.1 wppm, is again by brittle, inter-granular fracture along the weld interface. In contrast, at $C_L^0$ below 0.1 wppm, necking occurs within the softer 690 alloy at a location away from the weld line; a cup and cone failure was observed with micro-void coalescence evident in the central cup. In broad terms, we conclude that the presence of low concentrations of hydrogen has only a very mild influence on the ductile failure of the notched and un-notched specimens, whereas a higher concentration of hydrogen significantly degrades the cleavage strength of the weld. This interpretation is made more precise by a finite element study, as reported in the following section.

Additional insight into the competition between cleavage and ductile fracture is obtained by measuring with the SEM the area fraction of fracture surface that exhibits brittle, inter-granular cracking. Representative sketches of the failed cross-section of the notched specimens are given in Fig. 5 for selected values of hydrogen concentration, and a plot of the area fraction of cleavage fracture versus $C_L^0$ is given in Fig. 6 for both notched and un-notched specimens. The dependence of area fraction of cleavage upon $C_L^0$ is very similar for both geometries, and a clear transition in response from cleavage to micro-void coalescence is noted at $C_L^0$ equal to 0.1. This characteristic response of area fraction of cleavage versus $C_L^0$ has direct practical benefit in a failure investigation: it gives guidance upon the hydrogen content within a failed specimen or structure.

## 5. Establishment of a failure criterion

We proceed to establish a failure criterion for the notched (and unnotched) specimens in the presence of hydrogen. Our overall goal is to generate a unique failure locus in terms of local tensile stress $\sigma_{22}$ versus local hydrogen concentration at the weld interface, and thereby rationalise the data shown in Fig. 3. But there is choice in the type of hydrogen concentration that dictates the strength: the degradation in strength may arise from the lattice concentration $C_L$, from the concentration at traps such as dislocations $C_T^{(\mathrm{d})}$, grain boundaries $C_T^{(\mathrm{gb})}$, or carbides $C_T^{(\mathrm{c})}$, or by some combination of the above.

First, consider the hydrogen concentration at grain boundary and carbide traps. Upon invoking Eqs. (1-4) we find that the carbide and grain boundary traps are both fully saturated i.e. $\theta_T^{(\mathrm{gb})} \approx 1$ and $\theta_T^{(\mathrm{c})} \approx 1$, for the range of $C_L^0$ values in our experiments[1]. We conclude that carbide and grain boundary traps at the bimaterial interface do not lead to the observed major drop in strength $\sigma_{\max}$ upon increasing $C_L^0$, recall Fig. 3. The lattice hydrogen and hydrogen trapped at dislocations are however potential sources of hydrogen embrittlement. Consequently, in the remainder of this paper we shall asses the relative significance of lattice hydrogen and dislocation traps in degrading the strength of the bimaterial interface.

### *5.1. Finite element analysis*

In order to determine a failure locus for a bimaterial interface, in terms of local tensile stress $\sigma_{22}$ versus any choice of local hydrogen concentration, a knowledge of $\sigma_{22}$ and of the local hydrogen concentration is required. The local lattice hydrogen concentration $C_L$ depends upon the local hydrostatic stress in accordance with Eq. (9), while $C_T^{(\mathrm{d})}$ follows from Eqs. (2-6), where the von-Mises plastic strain is taken as an input. We employ, an axi-symmetric, elastic-plastic FE model in order to calculate the stress and strain distribution of the notched specimens at failure, see Fig. 1a. The FE mesh consists of 1461 bilinear quadrilateral elements, and the mesh density is increased in the vicinity of the notch in order to determine accurately the stress and strain state at the notch root. Both elastic and plastic response

[1] In Eqs. (1-4) we assumed that $\beta = 6$ and $N_L = 8.46 \times 10^{28}$ m$^{-3}$ for BCC iron (Sofronis and McMeeking, 1989) and the trap binding energies for grain boundaries and carbides are $\Delta H^{(\mathrm{gb})} = -48$ kJ/mol and $\Delta H^{(\mathrm{c})} = -72$ kJ/mol (Novak et al., 2010), respectively.

for 690 alloy and LAS are defined by separate uniaxial tensile stress versus strain curves measured from un-notched monolithic specimens tested in air. The FE analysis assumes of $J_2$ flow theory, with isotropic hardening. The experimentally measured uniaxial stress versus strain curves were idealised as

$$\sigma = \begin{cases} E\varepsilon & \varepsilon \leq \sigma_y/E \\ \sigma_y + h\varepsilon^{\mathrm{p}} & \varepsilon > \sigma_y/E \end{cases} \tag{10}$$

where $E$ is the Young's modulus, $\varepsilon$ is the total strain, $\sigma_y$ is the yield strength and $h$ is the plastic hardening rate. The value of parameters that characterise the mechanical response of 690 alloy and LAS are tabulated in Table. 2. We assume that the hardening rate $h$ remains the same upon exposure to hydrogen in LAS and 690 alloy. In support of this assumption, we note that Wang et al. (2005) found hydrogen charging did not change the shape of the stress-strain curves of AISI-4135 high strength low alloy steel but only reduced the ductility due to the switch in failure mechanism.

*5.2. Failure locus*

In order to assess the roles of $C_L$ and $C_T^{(\mathrm{d})}$ hydrogen embrittlement we begin by attempting to construct a unique failure locus of $\sigma_{22}$ versus $C_L$ from the measured data. In a similar manner we shall assess whether the experimental data suggests a unique failure locus of $\sigma_{22}$ versus $C_T^{(\mathrm{d})}$. Our strategy of seeking a failure locus follows that of Wang et al. (2005) and Ayas et al. (2013), and can be outlined as follows. Consider a notched specimen which has been charged to a selected value of $C_L^0$. The stress distribution $\sigma_{22}(x_1)$ along the net section is determined by elasto-plastic FE analysis, at an overall net-section stress level given by the observed value of $\sigma_{\max}$. In addition, the hydrostatic stress distribution $\sigma_h(x_1)$ is deduced from the FE analysis. For the un-notched specimens the stress state is uniform prior to any necking and $\sigma_{22} = \sigma_{\mathrm{net}}$. We proceed to calculate the distribution of $C_L(\sigma_h)$ as a function of position from Eq. (9) with $T = 298$K and $V_H = 2.1 \times 10^{-6}$ m$^3$/mol: in all the tests, the test time exceeded the diffusion time of lattice hydrogen in LAS which justifies the use of Eq. (9). Then we plot trajectories of $\sigma_{22}$ versus $C_L$ by treating position as an intrinsic variable, for any prescribed value of $C_L^0$ in the notched tests, see Fig. 7. For the un-notched specimens, the hydrostatic stress is uniform, and so we obtain uniform distributions of $\sigma_{22} = \sigma_{\mathrm{net}}$ and $C_L(x_1)$ from Eq. (9). Consequently, failure of un-notched specimens are represented by points in $\sigma_{22}$ versus $C_L$

space, see Fig. 7. A failure locus can be constructed in $\sigma_{22}$ versus $C_L(\sigma_h)$ space by drawing an outer envelope to the individual trajectories for notched specimens. In similar fashion, a failure locus for the un-notched specimens is constructed by connecting the points which represent the failure state of un-notched specimens in $\sigma_{22}$ versus $C_L$ space. We observe from this procedure that the locus for the un-notched specimens lies significantly below that deduced for the notched specimens. A pronounced size effect is evident and this will be explained further below.

A similar construction has been attempted for the case of trapped hydrogen: $\sigma_{22}$ is plotted versus $C_T^{(\mathrm{d})}$ for each notched and un-notched sample at failure in Fig. 8. The distribution $C_T^{(\mathrm{d})}(x_1)$ is calculated from Eq. (2-6), by making use of the known distribution of $\varepsilon^{\mathrm{p}}(x_1)$ and the lattice parameter $a = 0.287$ nm. Note that the plastic strain $\varepsilon^{\mathrm{p}}$ is deduced from the FE analysis for the notched samples while it is given immediately from Eq.(10) for the un-notched specimens.

We have considered two extreme values of dislocation trap binding energy in order to bound the behaviour. In Fig. 8a and Fig. 8c the results are presented for the choice $\Delta H^{(\mathrm{gb})} = -18$ kJ/mol for notched and un-notched specimens, respectively while in in Fig. 8b and Fig. 8d, $\Delta H^{(\mathrm{gb})} = -36.4$ kJ/mol is assumed for notched and un-notched specimens, respectively. Upon plotting $\sigma_{22}$ at failure against $C_T^{(\mathrm{d})}$ for the prescribed values of $C_L^0$, we obtain failure trajectories for the notched specimens at different hydrogen concentrations $C_L^0$; see Fig. 8a and Fig. 8b. Now consider the un-notched specimens. The data points in Fig. 8c and Fig. 8d represent the values of $(\sigma_{22} = \sigma_{\max}, C_T^{(d)})$ at failure since $\varepsilon^{\mathrm{p}}$ and $\sigma_{22}$ are uniform.

First, observe that the choice of $\Delta H^{(\mathrm{gb})}$ does not change the relative location of trajectories in the notched tests, and data-points in un-notched tests. An outer failure envelope of trajectories (for the notched specimens) cannot be identified in $\sigma_{22}$ versus $C_T^{(\mathrm{d})}$ space in Figs. 8a and 8b. Likewise, the relative positioning of the data-points in Figs. 8c and 8b does not allow for the construction of a unique failure locus. We conclude that the data can only be rationalised in terms of a failure locus in $\sigma_{22}$ versus $C_L$ space.

## 6. Weakest link statistics

It remains to explore possible reasons for the weaker response of the un-notched specimens compared to the notched ones, recall Fig. 7. When $C_L^0$ exceeds 0.1 wppm, hydrogen induces brittle inter-granular failure. For such

brittle solids, failure initiates from the largest inherent flaw, and probability of having large flaws increases with the size of stressed volume. Weakest link theories of strength, such as Weibull theory, attempt to account for such size effects. Moreover, introducing the concept of failure probability as opposed to a deterministic failure criterion also explains the scatter observed in the strength measurements. Here, we proceed to make use of Weibull statistics in an attempt to

(i) to rationalise the scatter in measured $\sigma_{\rm net}$ data, and
(ii) bring into alignment the notched and un-notched strength strength data of bimaterials as reported above.

*6.1. Analysis of scatter in strength*

In order to to rationalise the scatter in strength, we performed six tensile tests on identical un-notched specimens, all of which were continuously charged to $C_L^0 = 0.25$ wppm during the test, see Fig. 3. Although the number of repeated tests is insufficient for a rigorous statistical analysis, we nevertheless proceed to calculate the parameters of Weibull distribution from this batch of tests. We define the survival probability for each specimen as

$$P_s = \frac{n}{N+1} \tag{11}$$

where $n$ is the rank a given specimen upon ordering the specimens in a descending order of $\sigma_{\rm net}$ while $N = 6$ is the total number of un-notched specimens. Recall that the probability of survival $P_s$ for a component of volume $V$ can be estimated from the distribution of maximum tensile principal stress $\sigma_{22}(x_i)$[2] for the uniaxial loading imposed, according to the Weibull relation

$$P_s(\sigma_{ij}, V) = \exp\Big\{ -\frac{1}{V_0}\int_V \Big(\frac{\sigma_{22}}{\sigma_0}\Big)^m dV \Big\}. \tag{12}$$

Here, the Weibull modulus $m$ gives the variability of strength whereas $\sigma_0$ is a measure of average strength for a volume $V$ equal to a reference volume $V_0$. We calibrate the Weibull model by taking $V_0$ to be the volume of the

[2]For all the cases analysed here the maximum principal stress is approximately equal to $\sigma_{22}$.

un-notched specimens for which case the Weibull relation Eq. (12) reduces to

$$P_s = \exp\left\{-\left(\frac{\sigma_{\max}}{\sigma_0}\right)^m\right\}. \tag{13}$$

We emphasise that Eq. (13) gives the distribution in strength for a large population of nominally identical tensile specimens, subjected to identical charging conditions. Now in order to find the values of $m$ and $\sigma_0$ we take the natural logarithm of both sides twice in Eq. (13) and obtain

$$\ln\left[\ln\left(\frac{1}{P_s}\right)\right] = m\ln\left(\frac{\sigma_{\max}}{\sigma_0}\right). \tag{14}$$

The data from the six repeat tests is plotted in Fig. 9 and a best fit to the data suggests that $m = 3.4$ and $\sigma_0$ equals 346 MPa.

*6.2. Prediction of the size effect*

In the previous section we extracted the parameters associated with the Weibull distribution of strength by correlation with the scatter in repeat tests. Here, we make use of Weibull theory to reconcile the notched and un-notched strengths at $C_L^0 > 0.1$ wppm. We proceed by modifying Weibull theory to account for the fact that failure occurs from flaws on the interface between LAS and 690 alloy; consequently, the probability of failure is a function of stressed area rather than stressed volume. The survival probability of notched bimaterial specimen with a cross-sectional area $A$ becomes

$$P_s(A) = \exp\left\{\frac{1}{A_0}\int_A -\left(\frac{\sigma_{22}(x_i)}{\sigma_0(x_i)}\right)^m dA\right\}, \tag{15}$$

where $A_0$ is taken to be the cross sectional area of the un-notched bars, and $\sigma_{22}(x_i)$ is the tensile stress at any location $x_i$ on the interface. It is worth emphasising here that the representative strength $\sigma_0(x_i)$ is dependent upon local hydrogen concentration and so can vary with position $x_i$.

Equation (15) is valid for a perfectly flat weld interface but in reality the interface is wavy, see Fig. 10, and so some further modification is needed to the theory. Much of the interface is located either above or below the net-section of the notched specimen in a random manner, as illustrated in Fig. 10a. It is only the fraction of the net-section on which the interface

resides that is prone to failure. In order to account for this reduction in area fraction that is prone to failure, we modify Eq. (15) to the form

$$P_s(A) = \exp\left\{ \frac{1}{A_0} \int_A -\left( \frac{\sigma_{22}(x_i)}{\sigma_0(x_i)} \right)^m f dA \right\}, \tag{16}$$

where $f$ represents the fraction of the net section of the specimen that is intersected by the wavy interface. Our aim is to determine the value of $f$ that reconciles the notched and un-notched data.

To achieve this we need to know values of $m$ and $\sigma_0$ as a function of $C_L$ to use in Eq. (16). This is done as follows using the un-notched. data. We assume $m = 3.4$ as deduced from the scatter in the un-notched strength, see section 6.1 and extract the dependence $\sigma_0(C_L)$ as follows. The data from the un-notched (and notched) tests are too limited to perform a full Weibull analysis, and so we arbitrarily choose a survival probability of $P_s = 0.1$ at failure for all tests[3]. Now make use of Eq. (16) for the un-notched tests and take $f \equiv 1$ since the interface is uniformly stressed. With $A_0$ equal to the net-section area, and $\sigma_{22} = \sigma_{\max}$, Eq. (16) reduces to

$$P_s = \exp\left\{ -\left( \frac{\sigma_{\max}}{\sigma_0} \right)^m \right\}. \tag{17}$$

The data plotted in Fig. 3 gives $\sigma_{\max}$ as a function of $C_L^0$, and Eq. (17) gives directly $\sigma_0$ as a function of $C_L^0$. But we seek $\sigma_0$ as a function of the lattice hydrogen concentration $C_L$. To do so we invoke Eq.(9) with $\sigma_h = \sigma_{\max}/3$. The resulting calibration is given in Fig. 11a.

The final step is to use Eq. (16) to calculate $\sigma_{\max}$ for the notched specimens as a function of $C_L^0$ for selected values of $f$ as follows. Choose a value of $C_L^0$ corresponding to a particular test on a notched specimen. Then, perform a finite element analysis to obtain $\sigma_{22}(x_i)$ and $\sigma_h(x_i)$ on the net-section, at a prescribed value of $\sigma_{\max}$. The corresponding distribution $C_L(x_i)$ is obtained from Eq.(9), by making use of $\sigma_h(x_i)$. The value of $P_s$ is determined via Eq. (16), making use of $\sigma_0(C_L)$ from Fig. 11a and the selected value of $f$. We iterate with the value of $\sigma_{\max}$ until we obtain $P_s = 0.1$, to within an accuracy of 1 %. The above procedure is repeated for other values of $C_L^0$ (corresponding to the notched tests), and the predictions of $\sigma_{\max}$ versus $C_L^0$

[3]A side check reveals that our subsequent conclusions are relatively insensitive to this choice of $P_s$.

are plotted in Fig. 11b. The predictions are brought into agreement with the measurements by assuming $f = 0.1$.

## 7. Conclusions

We have explored the degradation in failure strength due to the presence of hydrogen for a weld interface between 690 alloy and A533B low alloys steel. A negligible degree of embrittlement is observed when $C_L^0 < 0.1$ and the bimaterial fails by micro-void coalescence. In contrast, upon charging the specimens to higher levels of hydrogen a significant drop in strength is observed and the fracture surface exhibits predominantly inter-granular cracking. A failure locus has been determined for notched and un-notched specimens using the axes of lattice hydrogen concentration and maximum principle stress. The role of trapped hydrogen appears to be negligible in dictating the fracture strength.

Significant scatter in the strength is observed for severely charged specimens and this has been rationalised by appealing to Weibull theory with a Weibull modulus of $m = 3.4$. Moreover, this same value of Weibull modulus reconciles the relative strength of notched and un-notched specimens by taking into account a stressed volume effect and the wavy nature of the welding interface. This value of $m$ is much smaller than the value of $m = 30$ found in a previous study for a monolithic high strength steel (Ayas et al., 2013). An immediate implication is the anticipation of a sharp drop of strength for large structural bimaterial components that are exposed to a hydrogen concentration above a threshold value. Since hydrogen absorption during the welding operation is a common phenomenon, a subsequent post weld heat treatment is a viable precaution to remove the hydrogen, as done in industrial practice.

## Acknowledgements

The authors wish to acknowledge Hiroshi Kanasaki, Naoki Ogawa and Yasuhiro Iwamura for their valuable comments and the Mitsubishi Heavy Metal Industries for the financial support.

## References

Ayas, C., Deshpande, V. S., Fleck, N. A., 2013. A fracture criterion for the notch strength of high strength steels in the presence of hydrogen, to appear in *Journal of the Mechanics and Physics of Solids* .

Blach, J., Falat, L., Sevc, P., 2011. The influence of hydrogen charging on the notch tensile properties and fracture behaviour of dissimilar weld joints of advanced crmov and crnimo creep-resistant steels. Engineering Failure Analysis 18 (1), 485 – 491.

Lee, C.-H., Chang, K.-H., 2012. Temperature fields and residual stress distributions in dissimilar steel butt welds between carbon and stainless steels. Applied Thermal Engineering 4546 (0), 33 – 41.

Novak, P., Yuan, R., Somerday, B. P., Sofronis, P., Ritchie, R. O., 2010. A statistical, physical-based, micro-mechanical model of hydrogen-induced intergranular fracture in steel. Journal of the Mechanics and Physics of Solids 58 (2), 206 – 226.

Oriani, R. A., 1970. The diffusion and trapping of hydrogen in steel. Acta Metallurgica 18 (1), 147 – 157.

Rao, N. V., Reddy, G. M., Nagarjuna, S., 2011. Weld overlay cladding of high strength low alloy steel with austenitic stainless steel structure and properties. Materials and Design 32 (4), 2496 – 2506.

Satyanarayana, V. V., Reddy, G. M., Mohandas, T., 2005. Dissimilar metal friction welding of austeniticferritic stainless steels. Journal of Materials Processing Technology 160 (2), 128 – 137.

Sireesha, M., Shankar, V., Albert, S. K., Sundaresan, S., 2000. Microstructural features of dissimilar welds between 316ln austenitic stainless steel and alloy 800. Materials Science and Engineering: A 292 (1), 74 – 82.

Sofronis, P., McMeeking, R. M., 1989. Numerical analysis of hydrogen transport near a blunting crack tip. Journal of the Mechanics and Physics of Solids 37 (3), 317 – 350.

Wang, M., Akiyama, E., Tsuzaki, K., 2005. Effect of hydrogen and stress concentration on the notch tensile strength of aisi 4135 steel. Materials Science and Engineering A 398 (1-2), 37 – 46.

Table 1: Charging conditions employed in this study in terms of the charging environment and the applied current density $J$. The environmental hydrogen concentration $C_L^0$ corresponding to each of these charging conditions is also indicated in the table.

| Charging environment | $J$ (mA/cm$^2$) | $C_L^0$ (wppm) |
|---|---|---|
| air | - | 0 |
| 1/3M $H_3BO_3$ +1/30M KCl | 0 | 0.07 |
| 1/3M $H_3BO_3$+1/30M KCl | 2 | 0.11 |
| 1/3M $H_3BO_3$+1/30M KCl | 4 | 0.13 |
| 1/3M $H_3BO_3$+1/30M KCl | 10 | 0.15 |
| 1/3M $H_3BO_3$+1/30M KCl+1/100M Thiourea | 10 | 0.25 |

Table 2: Material constants of Eq. (10) for the LAS and 690 alloy.

| Material | $E$ (GPa) | $\sigma_y$ (MPa) | $h$ (MPa) | $\nu$ |
|---|---|---|---|---|
| LAS | 210 | 532 | 2517 | 0.3 |
| 690 alloy | 209 | 397 | 2533 | 0.3 |

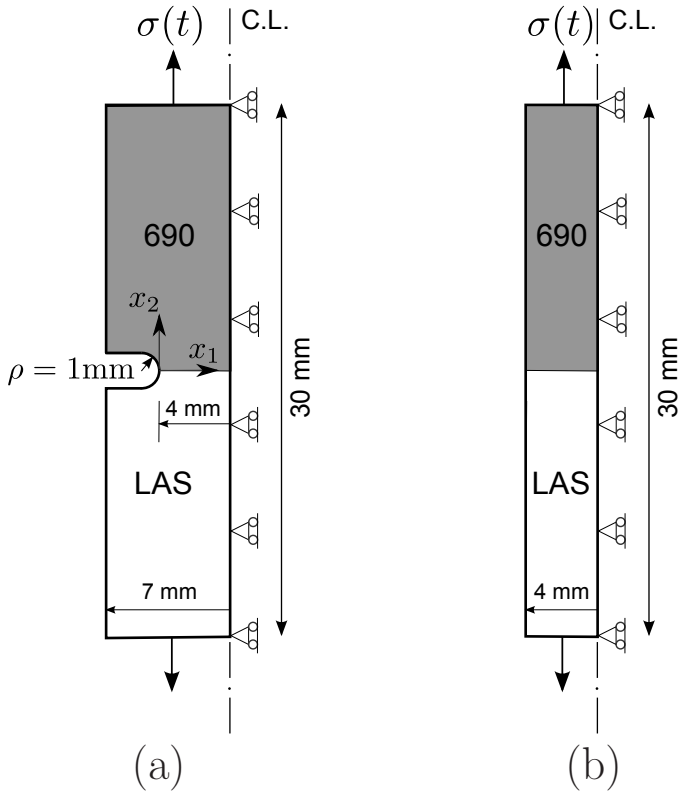


Figure 1: Sketch of the gauge sections of the (a) notched and (b) un-notched specimens used in this study. The boundary conditions applied in the FE analysis of these specimens are also indicated.

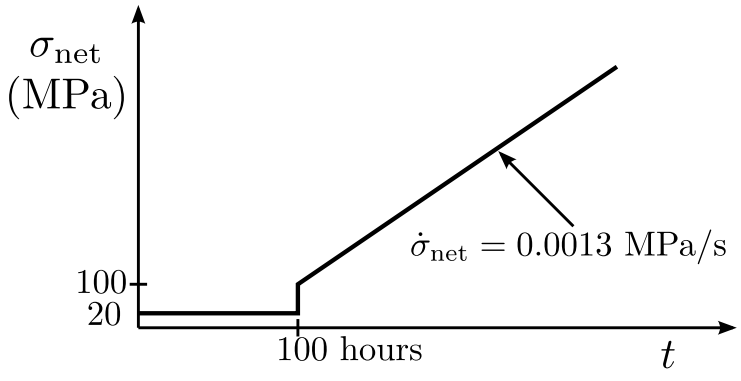


Figure 2: The loading history in terms of the tensile stress $\sigma_{\text{net}}$ versus time that he tensile specimens are subjected to in the charging environment.

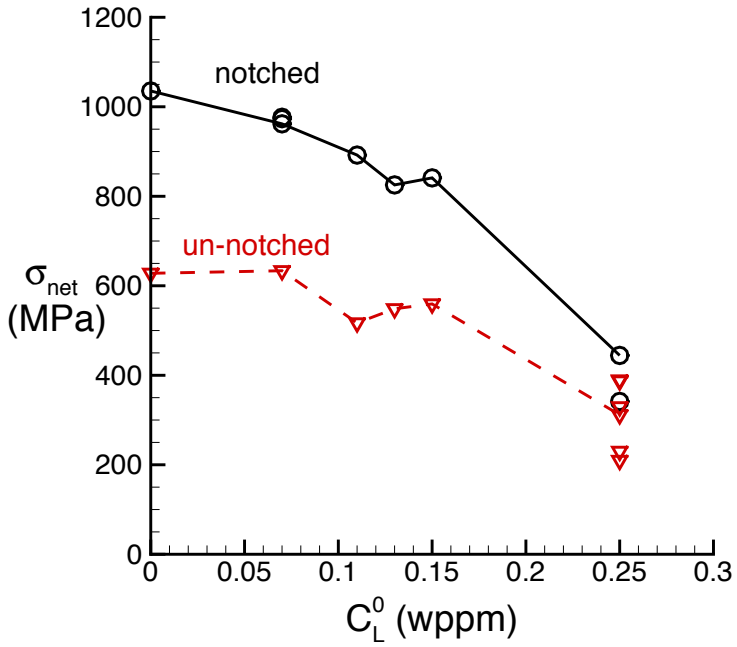


Figure 3: Measured net-section strength $\sigma_{\max}$ of notched and un-notched specimens as a function of the hydrogen concentration $C_L^0$ in the charging environment.

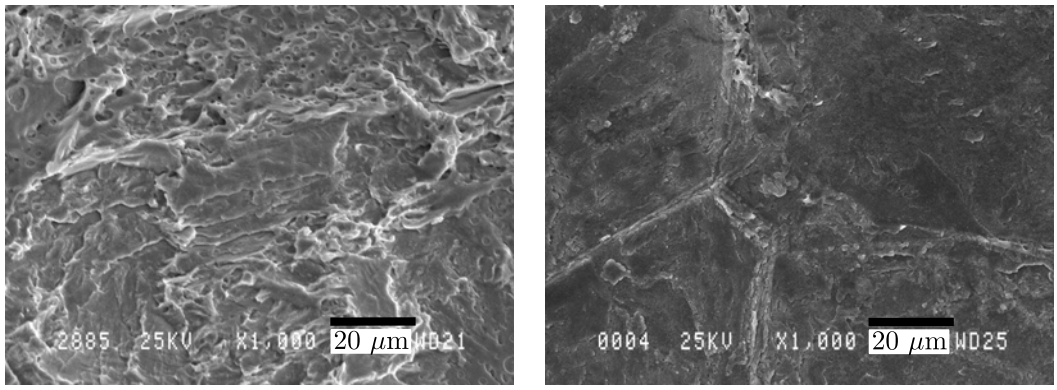


(a) (b)

Figure 4: Scanning electron micrographs of the fracture surfaces of notched specimens charged to (a) $C_L^0 = 0.07$ wppm and (b) $C_L^0 = 0.25$ wppm.

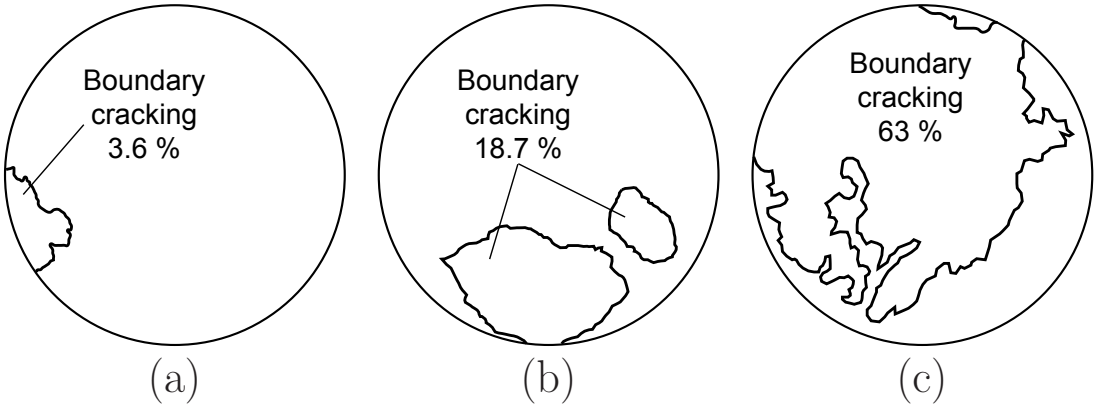


Figure 5: Sketches of the fracture surfaces of the notched specimens charged to (a) $C_L^0 = 0.07$ wppm, (b) $C_L^0 = 0.15$ wppm and (c) $C_L^0 = 0.25$ wppm. The sketches show regions where brittle inter-granular boundary cracking was observed.

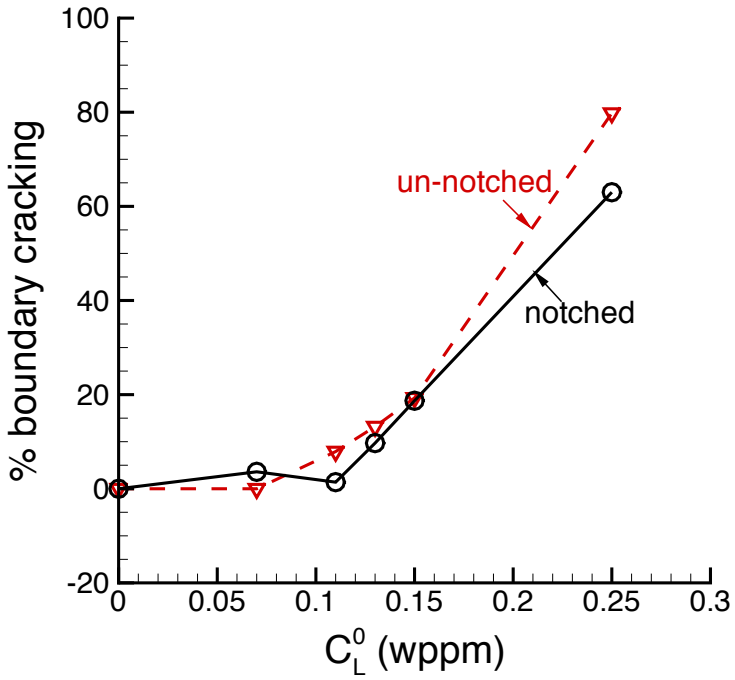


Figure 6: Percentage of the fracture surface that exhibits features of inter-granular boundary cracking as a function of $C_L^0$. Data for both notched and un-notched specimens is shown.

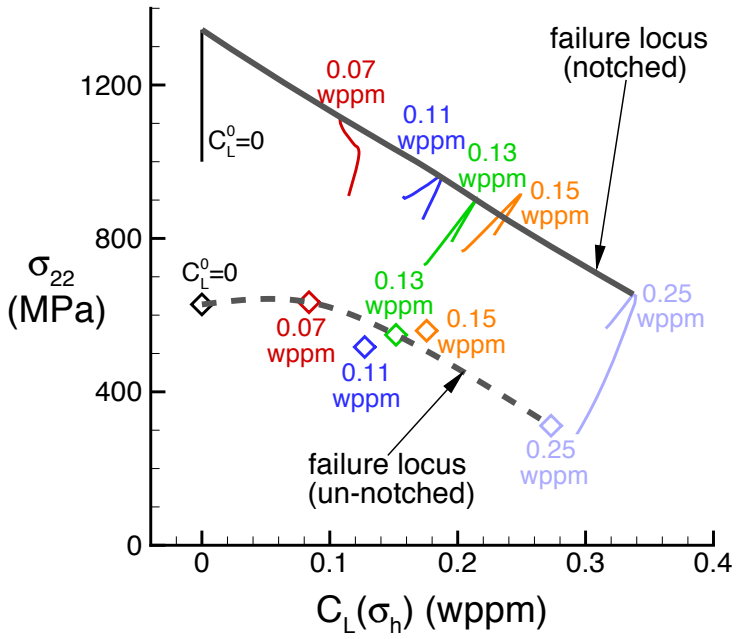


Figure 7: Predictions of the trajectories of the local tensile stress $\sigma_{22}$ as a function of the diffusible/lattice hydrogen concentration $C_L$ for tests on both the notched and un-notched specimens. Since the stress state within the un-notched specimens is uniform the trajectories collapse to a single point for each test. The failure locus deduced from the data is indicated in each case.

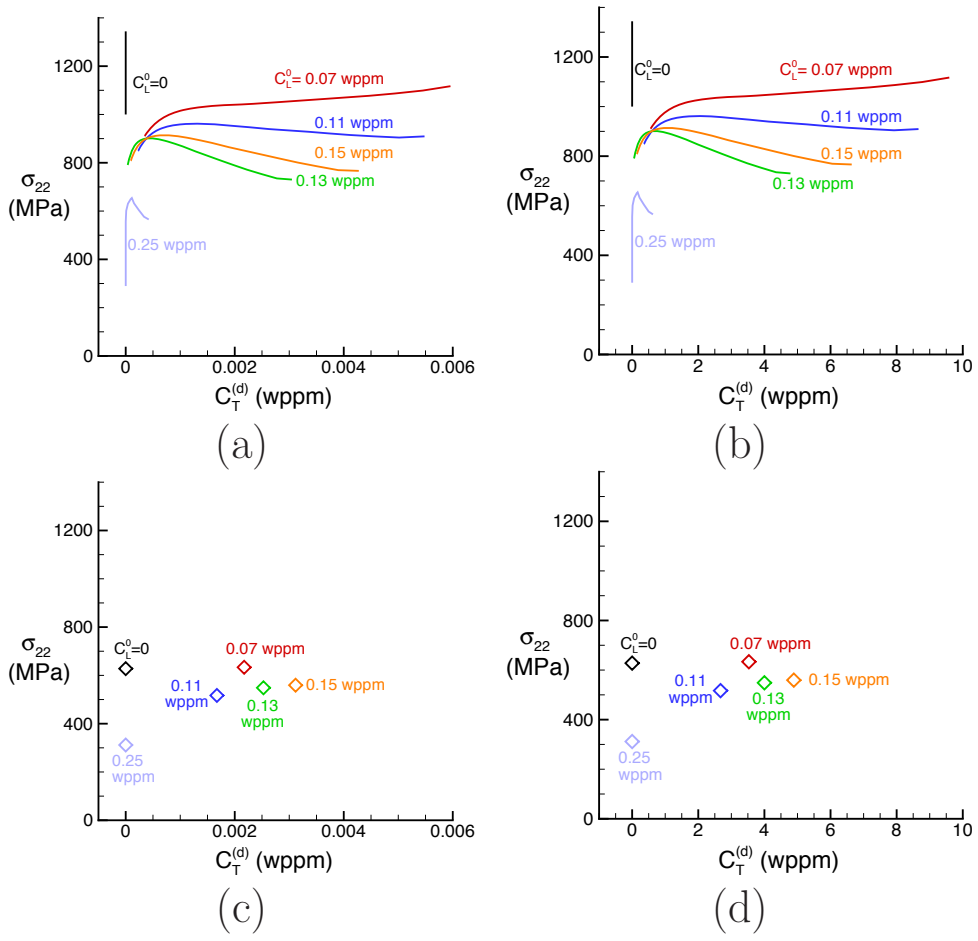


Figure 8: Predictions of trajectories of the local stress $\sigma_{22}$ versus hydrogen concentration $C_T^{(d)}$ trapped at the dislocations for the notched and un-notched specimens. In (a) and (b) predictions are shown for the notched specimens assuming $\Delta H^{(\mathrm{gb})} = -18$ kJ/mol and $-36.4$ kJ/mol, respectively while in (c) and (d) the data points correspond to the un-notched specimens with again $\Delta H^{(\mathrm{gb})} = -18$ kJ/mol and $-36.4$ kJ/mol, respectively.

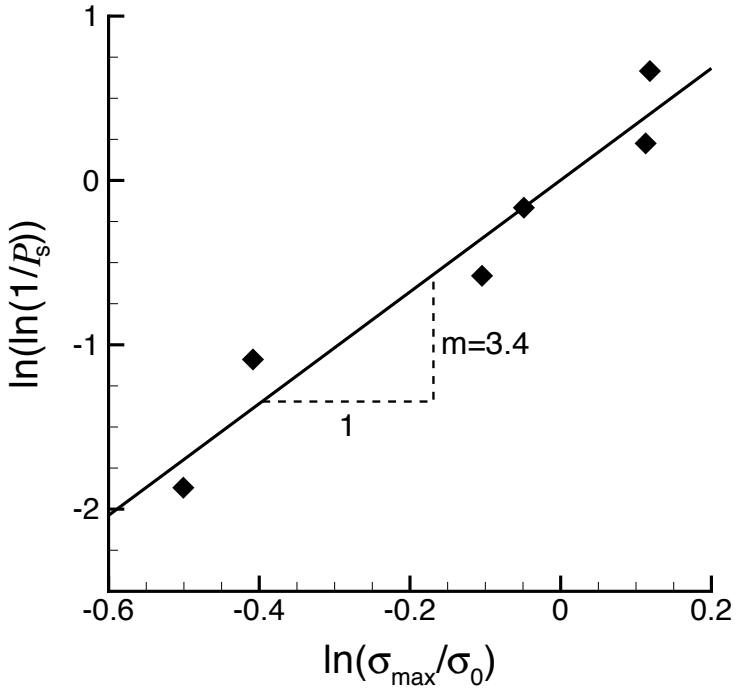


Figure 9: Probability of survival $P_s$ calculated from repeat tests performed on un-notched specimens with $C_L^0 = 0.25$ wppm as a function of the measured strength $\sigma_{\max}$. The data is plotted such that the Weibull modulus $m$ can be readily extracted using Eq. (14).

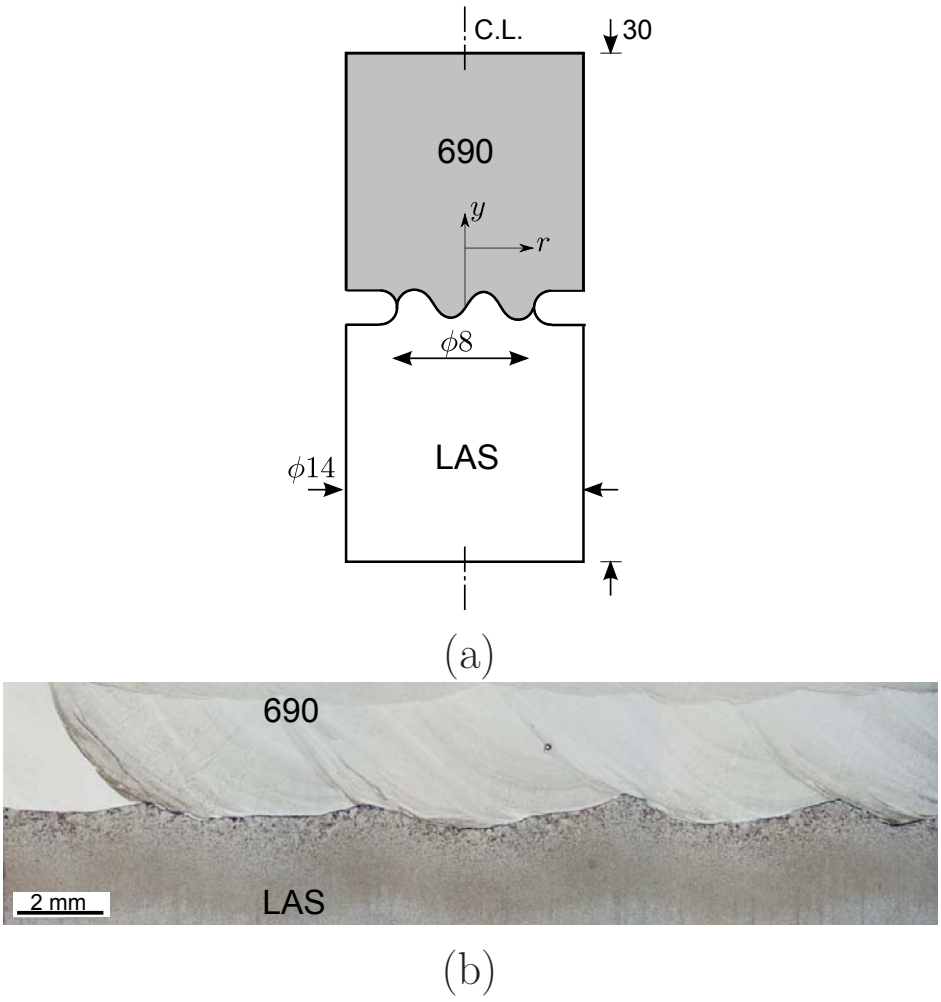


Figure 10: (a) Sketch of the wavy weld interface between the 690 alloy and LAS with all dimensions given in mm. (b) Optical micrograph of the weld interface.

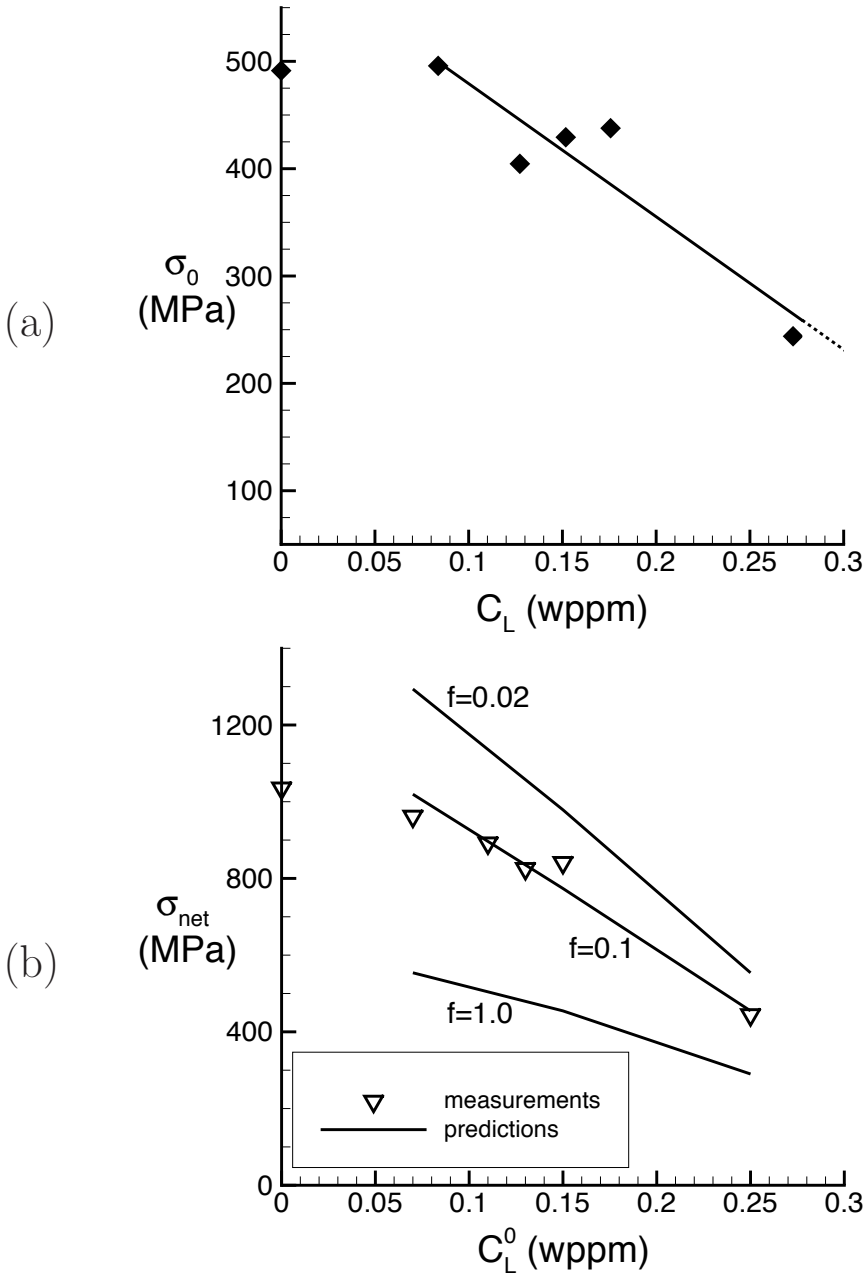


Figure 11: (a) The values of $\sigma_0$ as a function of $C_L$ as inferred from the un-notched specimen tests. (b) The measured and predicted net-section strength $\sigma_{\max}$ for the notched specimens. Predictions are shown for three selected values of the parameter $f$ that characterises the waviness of the weld interface.